Neuroradiology (2021) 63:609–617
https://doi.org/10.1007/s00234-020-02549-y

INTERVENTIONAL NEURORADIOLOGY

Delineability and anatomical variations of perforating arteries from normal vertebral artery on 3D DSA: implications for endovascular treatment of dissecting aneurysms

Shuichi Tanoue[1] · Hidenori Endo[2] · Masafumi Hiramatsu[3] · Yuji Matsumaru[4] · Yasushi Matsumoto[5] · Kenichi Sato[5] · Wataro Tsuruta[6] · Masayuki Sato[4] · Masaru Hirohata[7] · Toshi Abe[1] · Hiro Kiyosue[8] · on behalf of the JSNET VADA study group

Received: 26 May 2020 / Accepted: 1 September 2020 / Published online: 21 September 2020

Abstract

Background and Purpose Endovascular trapping of the vertebral artery dissecting aneurysms (VADAs) carries a risk of medullary infarction due to the occlusion of the perforating arteries. We evaluated the detectability and anatomical variations of perforating arteries arising from the vertebral artery (VA) using three-dimensional DSA.

Methods In 120 patients without VA lesions who underwent rotational vertebral arteriography, the anatomical configurations of perforating arteries from the VA were retrospectively evaluated on the bi-plane DSA and reconstructed images to reach the consensus between two experienced reviewers. The images were interpreted by focusing on the numbers and types of perforating arteries, the relationships between the number of perforators and the anatomy of the VA and its branches.

Results Zero, 1, 2, 3, 4, and 6 perforators were detected in 2, 51, 56, 9, 1, and 1 patient, respectively (median of 2 perforators per VA). The 200 perforators were classified into 146 terminal and 54 longitudinal course types and into 32 ventral, 151 lateral, and 17 dorsolateral distribution types. All ventral type perforators were also terminal type. In contrast, the longitudinal type was seen in 28.5% of lateral types and in 65% of dorsolateral types. Regarding the difference in the origin of the posterior inferior cerebellar artery (PICA), non-PICA type VAs gave off larger number of perforators than the other types of VAs.

Conclusions Non-PICA type VAs give off a significantly larger number of perforators than other types, indicating that the trapping of non-PICA type VAs is associated with a risk of ischemic complications.

Keywords Vertebral artery · Perforating artery · 3D DSA · Anatomical variation

Introduction

Intracranial vertebral artery dissecting aneurysms (VADAs) are associated with acute ischemic stroke, subarachnoid hemorrhage, and other neurological symptoms [1]. A ruptured VADA is often followed by rebleeding, resulting in severe clinical outcomes in the acute stage [2, 3]. Therefore, early intervention is required to prevent rerupture of the VADA. Endovascular trapping of a ruptured VADA is a widely accepted treatment in obtaining reliable hemostasis by

✉ Shuichi Tanoue
tanoue_shuchi@med.kurume-u.ac.jp

[1] Department of Radiology, Kurume University School of Medicine, Kurume, Japan

[2] Department of Neurosurgery, Tohoku University Graduate School of Medicine, Sendai, Japan

[3] Department of Neurological Surgery, Okayama University Graduate School of Medicine, Dentistry and Pharmaceutical Sciences, Okayama, Japan

[4] Department of Neurosurgery, Faculty of Medicine, University of Tsukuba, Tsukuba, Japan

[5] Department of Neuroendovascular Therapy, Kohnan Hospital, Sendai, Japan

[6] Department of Endovascular Neurosurgery, Toranomon Hospital, Tokyo, Japan

[7] Department of Neurosurgery, Kurume University School of Medicine, Kurume, Japan

[8] Department of Radiology, Oita University Faculty of Medicine, Oita, Japan

protecting the ruptured site from both collateral and antegrade blood flow [4, 5]. However, endovascular trapping of the VADA carries a certain risk of medullary infarction [6–9] (Fig. 1). The ischemia in such cases has been considered to be caused by coiling and/or thrombosis of the orifice of unrecognized perforating arteries. However, these fine branches are not readily depicted on conventional vertebral angiography. Recent advances in angiographic technology have allowed us to evaluate the anatomy of the perforating arteries [10, 11].

The microanatomical features of perforating arteries arising from the cerebral artery have been previously evaluated by gross anatomical methods [12–14]. According to these reports, the vertebral artery (VA) gives off several perforating branches at the intracranial segment. However, the anatomical features of these perforating arteries have not been evaluated using radiological methods. In this study, the detectability and anatomical variations of perforating arteries arising from the VA were evaluated using reconstructed images of three-dimensional (3D) rotational vertebral angiography.

Materials and methods

Patients

This retrospective study was approved by the Institutional Review Board of Kurume University Hospital. Written informed consent was obtained from all patients before angiography; however, the need for informed consent for this study was waived because of the retrospective study design. From January 2016 to December 2017, 167 consecutive patients underwent 3D rotational vertebral angiography at two different major stroke centers equipped with the same angiographic

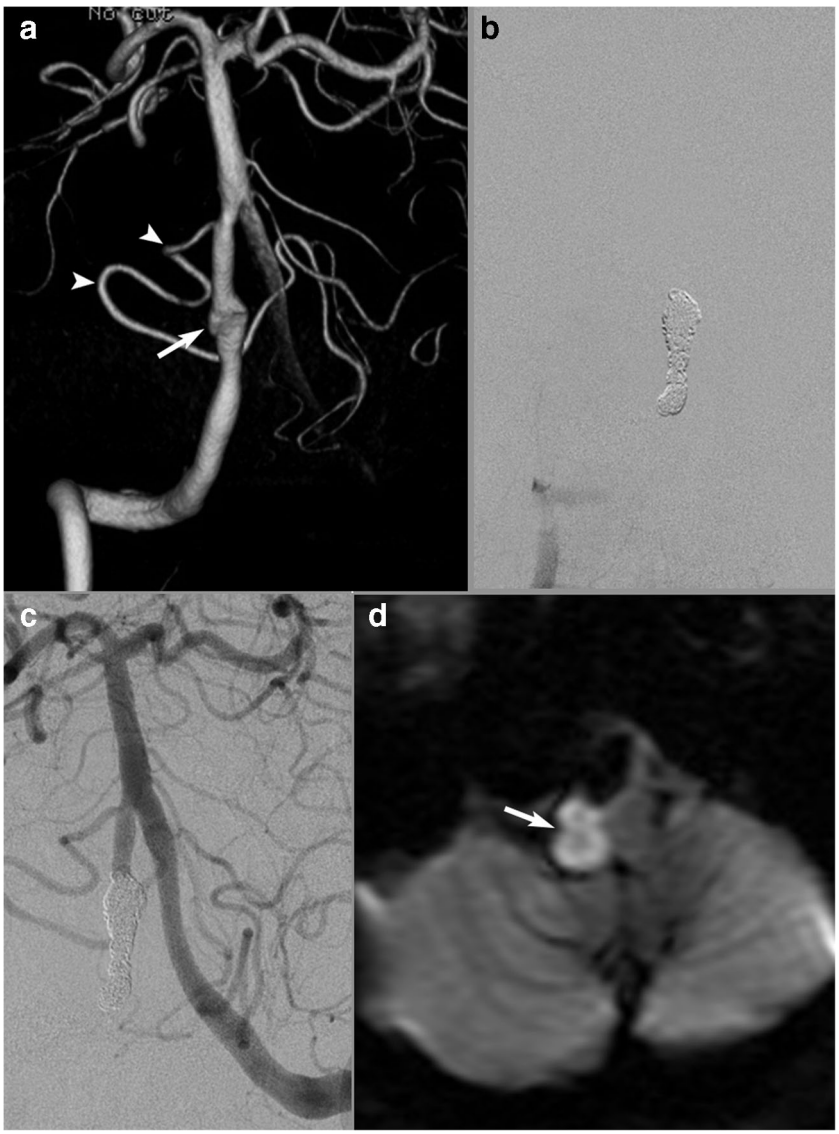

Fig. 1 Illustrative case with vertebral artery dissecting aneurysm (VADA) who presented medullary infarction after internal trapping. **a** Volume rendering image shows VADA at distal segment of the right vertebral artery (VA) (arrow). The right posterior inferior cerebellar artery (PICA) was originated from the distal side of VA (arrowheads). **b** Internal trapping using detachable microcoils was performed. Right vertebral arteriogram shows disappearance of VADA and stagnation of contrast material in proximal segment of right VA. **c** Contralateral vertebral arteriogram showed no retrograde filling of VADA and good patency of right PICA and basilar trunk. **d** Diffusion-weighted image 2 days after treatment revealed acute infarction in right half of medulla oblongata (arrow)

machine and workstation. Among them, 47 patients were excluded from this study because of the following factors, which prevented adequate evaluation of the normal angiographic anatomy: insufficient field of view on rotational angiography (26 patients), inappropriate image quality (3 patients), VA truncal lesions such as VA dissections or VA aneurysms (7 patients), arteriovenous fistulas involving VA perforators (9 patients), and brain tumors supplied by VA perforators (2 patients). The inappropriate image quality was due to the patient motion artifact (2 patients) and massive subarachnoid hematoma surrounding the medulla oblongata (1 patient). The remaining 120 patients (87 females, 33 males; age range, 11–83 years; mean, 57.9 years) were retrospectively evaluated. All 120 patients had undergone one-side vertebral arteriography; thus 120 vertebral arteries in total were analyzed. The underlying disease was an unruptured intracranial non-VA aneurysm in 57 patients, subarachnoid hemorrhage from a non-VA aneurysm or unknown etiology in 28, arteriovenous malformation in 8, intracranial dural arteriovenous fistula in 3, and other condition in 2.

Angiography

All angiography examinations were performed in an angiographic suite equipped with a biplane flat-panel detector system (Innova IGS 630; GE Healthcare, Milwaukee, WI, USA) in the two hospitals. The 4- or 5F-sized catheter was positioned at the proximal segment of the Vas, and non-ionic iodinated contrast material was injected through an automated injector. The imaging parameters for rotational angiography were set as follows: rotation angle, 200°; rotation speed, 40°/s; matrix size, 512 × 512 by 20-cm flat-panel detector; and non-ionic iodinated contrast material (Iopamidol 300) with a flow rate of 1.5 to 3.0 ml/s (total volume of 9–24 ml). The low flow rate injection was attempted for the non-dominant type VA having a small diameter. The raw data obtained from the biplane and rotational vertebral angiography were stored in the picture archiving and communication system (PACS) server in each hospital. The data were re-transferred to the workstation (Advantage Workstation VolumeShare; GE Healthcare) to compose the volume rendering reconstruction and multiplanar reconstruction with settings of 0.5- to 5.0-mm thickness and 1-mm interval.

Image interpretation

All angiographic and multiplanar reconstruction images were simultaneously evaluated by experienced neuroradiologist and endovascular neurosurgeon with 22 and 12 years of clinical experience to reach a consensus regarding the presence and anatomical configuration of the VA and perforating arteries. The baseline anatomical characteristics of the VA were examined with a particular focus on the dominancy of the VA in terms of its diameter and then classified into the dominant-side VA, the non-dominant-side, and equally sized VA. The existence of the origin of the anterior spinal artery (ASA), existence of the origin of the posterior inferior cerebellar artery (PICA), and distance from the VA union to the origin of the PICA were also evaluated. The dominancy of VA and the origin of ASA were evaluated based on the information from the retrograde filling of the contrast agent into the distal segment of the contralateral VA during the rotational vertebral arteriography.

The anatomical configuration of the perforating arteries was evaluated with a focus on the numbers and types of detectable perforators. The numbers of perforators were recorded in each patient. In addition, the relationships between the number of perforators and the baseline anatomy of the VA and its branches, including the origins of the anterior spinal artery (ASA) and the posterior inferior cerebellar artery (PICA), were evaluated. The types of perforating arteries were classified into terminal or longitudinal types depending on their course and into ventral, dorsal, or dorsolateral types depending on the location of their termination. The terminal type was defined as a perforator terminating at the same level of the medullary surface showing a short trunk, and the longitudinal type was defined as a perforator running longitudinally along the medullary surface (Fig. 2a). When the longitudinal type had multiple origins at the VA or other branches and these arterial roots join to be one longitudinal type perforator at the medullar surface, the numbers and locations of the origins were also recorded. The ventral type was defined as a perforator terminating at the ventral aspect of the medulla, the lateral type as one terminating at the lateral aspect, and the dorsolateral type as one terminating at the dorsolateral aspect (Fig. 2b). The distance between the VA union and the origin of the PICA or perforating arteries was also measured using the measurement tool on the workstation.

Statistical analysis

Statistical analysis was performed using the SPSS statistics version 21 (IBM, Armonk, NY, USA). The relationships between each type of VA and the numbers of detectable perforating arteries were statistically evaluated (Fisher's exact test). In addition, the differences among the types of perforating arteries were evaluated by comparing the distance between the VA and perforating arteries in each type (Mann–Whitney U test). A p-value of 0.05 or lower was considered to be statistically significant.

Results

The baseline anatomical characteristics of the VA were as follows: the dominant-side VA was present in 66 patients,

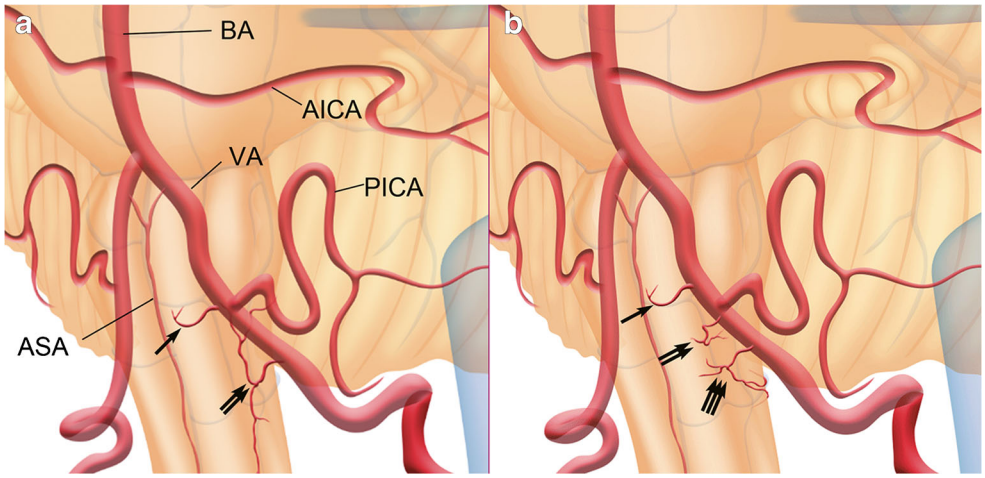

Fig. 2 Schematic drawings of anatomical configurations of perforating arteries (left anterolateral view of the medulla oblongata). **a** The terminal type was defined as a perforator terminating at the same level of the medullary surface, showing short trunk (arrow), and the longitudinal type was defined as a perforator running longitudinally along the medullary surface (double arrows). **b** The ventral type was defined as a perforator terminating at the ventral aspect of the medulla (arrow), the lateral type as one terminating at the lateral aspect (double arrows), and the dorsolateral type as one terminating at the dorsolateral aspect (triple arrows). AICA, anterior inferior cerebellar artery; BA, basilar artery; VA, vertebral artery; PICA, posterior inferior cerebellar artery; ASA, anterior spinal artery

the non-dominant-side VA was present in 10, and equally sized VAs were present in 44 patients. The ASA was given off from the ipsilateral VA in 69 patients, the contralateral VA in 31, and the bilateral VAs (double origin) in 11. The ASA was not detectable in the remaining nine patients. Therefore, 80 VAs served as the origin of the ASA and 40 VAs did not. The PICA originated from the intracranial VA in 87 patients, the extracranial VA in 26, and the anterior inferior cerebellar artery (AICA) in 7 (i.e., non–PICA-type VA) (Table 1).

Table 1 Baseline anatomical characteristics of the VA

	Number of patients
Dominancy of VA	
Dominant side	66
Equally sized	44
Non-dominant side	10
Origin of ASA	
Ipsilateral VA	69
Double origin	11
Contralateral VA	31
Not detectable	9
Origin of PICA	
Intracranial VA	87
Extracranial VA	26
AICA	7

VA vertebral artery, *ASA* anterior spinal artery, *PICA* posterior inferior cerebellar artery, *AICA* anterior inferior cerebellar artery

Zero, 1, 2, 3, 4, and 6 perforators were detected in 2, 51, 56, 9, 1, and 1 patient, respectively. Therefore, a total of 200 perforating arteries were detected (median, 2; interquartile range [IQR], 1–3). Among them, 146 perforating arteries were of the terminal type (Fig. 3a) and 54 were of the longitudinal type (Fig. 3b). In addition, 32 perforating arteries were of the ventral type, 151 were of the lateral type, and 17 were of the dorsolateral type (Fig. 4). All ventral type perforating arteries were of the terminal type. However, the lateral type perforating arteries comprised both the terminal type (71.5%) and longitudinal type (28.5%). Dorsolateral type perforating arteries were classified into the terminal type (35%) and longitudinal type (65%) (Fig. 5).

The left VA gave off zero to six perforators (median, 2 [IQR, 1–2]), and the right VA gave off one to four perforators (median, 2 [IQR, 1–2]) (Table 2). There was no significant difference in the number of detected perforating arteries according to the laterality of the VA ($p = 1.0000$). The dominant-side VA gave off zero to three perforating arteries (median, 2 [IQR, 1–2]), the non-dominant-side VA gave off zero to six perforating arteries (median, 2 [IQR, 1–2]), and the equal type VAs gave off one to three perforating arteries (median, 2 [IQR, 1–2]) (Table 2). There was no significant difference in the dominancy of the VA ($p = 0.6046$). The VAs containing the origin of the ASA gave off zero to three perforating arteries (median, 2 [IQR, 1–2]), whereas the VAs without the origin of the ASA gave off zero to six perforating arteries (median, 2 [IQR, 1–2]) (Table 2). There was no significant difference between the VAs with and without the origin of the ASA ($p = 1.0000$). Finally, the VAs with the PICA originating from the intracranial segment gave off zero to three perforating arteries (median, 1 [IQR, 1–2]), the VAs with the PICA originating from the

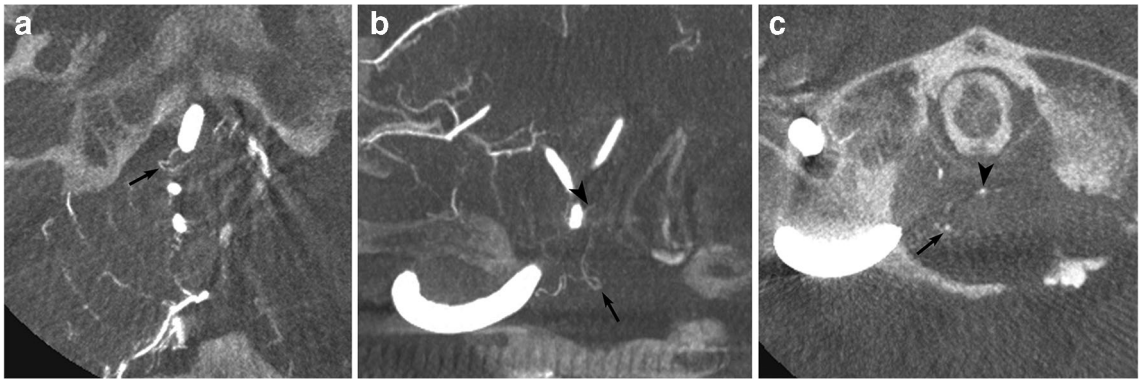

Fig. 3 Illustrative cases of detected perforating arteries. **a** A 60-year-old woman with a basilar top aneurysm. Axial reconstruction of a partial maximum intensity projection (MIP) image of rotational right vertebral angiography shows a perforating artery (arrow). This artery was classified as lateral and terminal type. **b** A 50-year-old man with a brain tumor. Coronal reconstruction of a partial MIP image of rotational right vertebral angiography shows a perforating artery (arrow). This artery was classified as lateral and longitudinal type. This artery rostrally anastomosed with a branch of the posterior inferior cerebellar artery (arrowhead). **c** Axial reconstruction image of identical rotational angiography shows same perforating artery running along the lateral surface of upper cervical spinal cord (arrow). Note the anterior spinal artery indicating anteromedian border of spinal cord (arrowhead). The ventral, lateral, and dorsolateral borders of the spinal cord and medulla could be assumed by positional relationships of these surrounding vessels

extracranial segment gave off one or two perforating arteries (median, 1 [IQR, 1–2]), and the VAs without the origin of the PICA (i.e., the PICA originated from the AICA) gave off one to six perforating arteries (median, 2 [IQR, 2–3]). The VAs without the origin of the PICA showed a significantly higher number of branching perforating arteries than those with the origin of the PICA ($p < 0.001$).

The longitudinal type perforating arteries had a single origin in 13 patients, double origins in 37, and triple origins in 4. The cumulative numbers of origins according to location were 56 from the VA, 39 from the PICA, and 4 from the C1 radicular artery.

The distance from the VA union to the origins of all perforating arteries ranged from 1.3 to 57.5 mm. The distance between the VA union and the origins of ventral type perforating arteries ranged from 1.3 to 57.5 mm (median, 5.1 mm [IQR, 5.6–10.375]), that between the VA union to the origins of lateral type perforating arteries ranged from 7.4 to 48.3 mm (median, 22.6 mm [IQR, 16.6–34.5]), and that between the VA union to the origins of dorsolateral type perforating arteries ranged from 33.2 to 48.0 mm (median, 41.1 mm [IQR, 33.2–46.8]). All distances between the VA union and each type of perforating artery showed a significant difference (Fig. 6).

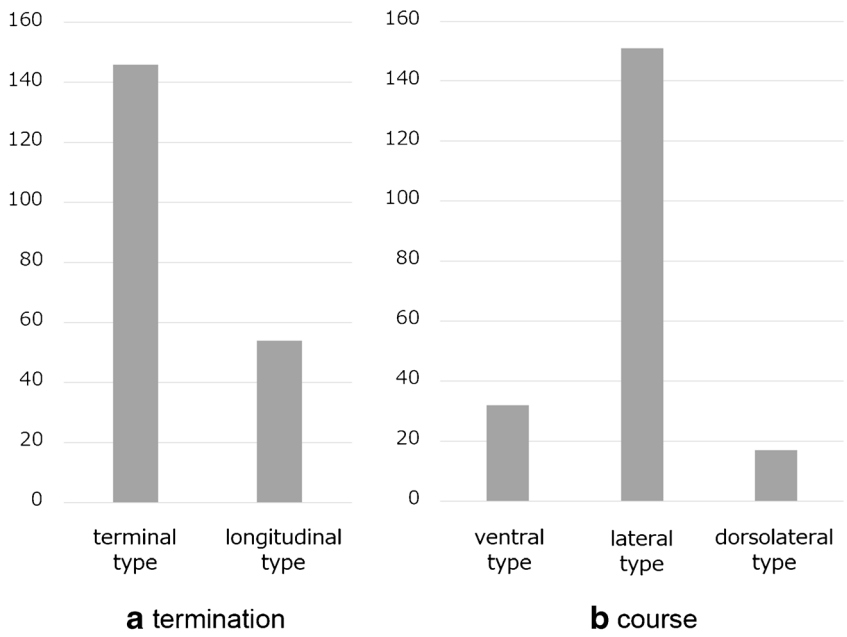

Fig. 4 Cumulative numbers of each type of all 200 perforating arteries. **a** Termination. **b** Course

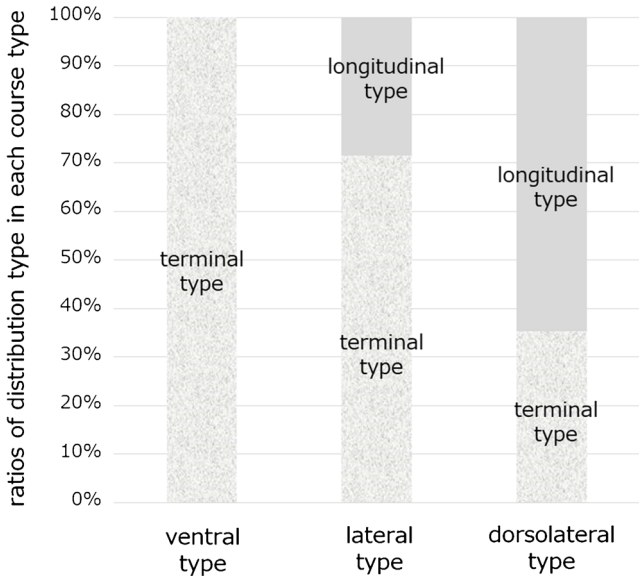

Fig. 5 Ratios of termination type in each course type

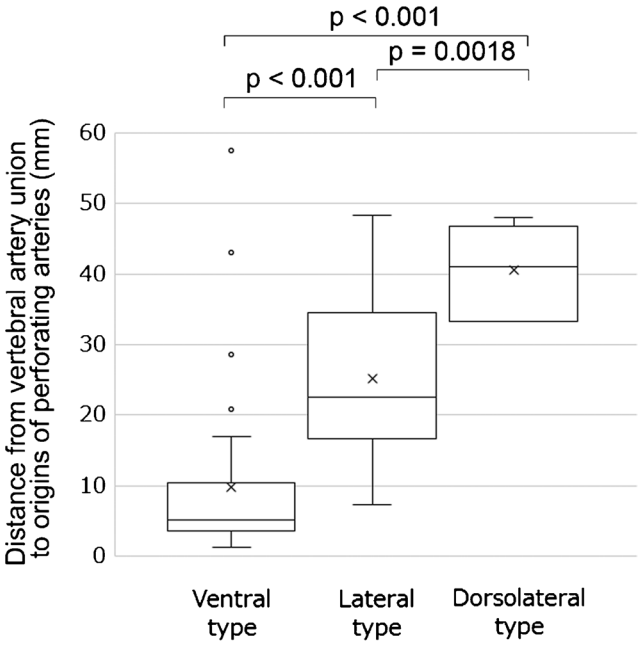

Fig. 6 Distance from the vertebral artery union to the origins of all perforating arteries

Discussion

Endovascular treatment for a ruptured VADA is traditionally performed to trap the dissected segment of the VA while avoiding occlusion of the origins of the PICA and ASA. The risk of medullary infarction due to occlusion of the perforating arteries has been previously discussed [6, 9, 15, 16]. According to these previous reports, the incidence of medullary infarction ranges from 19 to 47%. However, Endo et al. indicated that it is difficult to recognize ischemic complications in the acute stage of subarachnoid hemorrhage [6]. The ischemic tolerance of the perforating arteries is also difficult to assess by the balloon occlusion test. Therefore, clinicians must have adequate knowledge of the normal anatomy of the perforating arteries arising from the VA and the ability to detect them using conventional and 3D angiography. Recently, the flow-diverting stent placement has been reported as an alternative treatment technique to preserve the vertebral arterial flow as well as its branches [17–19]. The detectability of perforators might be an important information for the consideration of the flow-diverting stent placement.

The anatomy of the perforating arteries has been evaluated using gross anatomical methods [13, 14, 20–22]. However, the perforators from the VA have not been fully discussed. Marinkovic et al. evaluated the perforating arteries from the

Table 2 Relationships between VA branch types and numbers of detectable perforators

Anatomical types of VA	Number of patients in each detectable number of perforating arteries								*p*-values (Fisher's exact test)
	Detectable number of perforating arteries						Median number of perforators	IQR	
	0	1	2	3	4	6			
Left VA	2	37	39	6	0	1	2	1–2	1.0000
Right VA	0	14	17	3	1	0	2	1–2	
Dominant-side VA	1	30	35	2	0	0	2	1–2	0.6046
Equal type VA	1	17	20	4	1	1	2	1–2	
non-dominant-side VA	0	4	3	3	0	0	2	1–2	
VA with origin of ASA	1	36	40	3	0	0	2	1–2	1.0000
VA without origin of ASA	1	15	16	6	1	1	2	1–2	
VA with PICA originated from intracranial segment	2	45	37	3	0	0	1	1–2	<0.001
VA without PICA (non–PICA-type VA)	0	2	16	6	1	1	2	2–3	
VA with PICA originated from extracranial segment	0	4	3	0	0	0	1	1–2	

VA vertebral artery, *ASA* anterior spinal artery, *PICA* posterior inferior cerebellar artery, *IQR* interquartile range

VA and its side twigs [13]. In their study, the perforators that were given off from the VAs ranged in number from 1 to 3 (mean, 1.2) and in diameter from 210 to 520 μm. In the present series, the median number of detectable perforating arteries in all VAs was 2, which is consistent with the abovementioned anatomical study. In addition, only three (1.8%) patients were excluded from the original 167 cohort due to the inadequate image quality; the two of them was due to the patient motion artifact, and the remaining one was due to the massive hematoma. Our results indicated that the reconstructed images from the 3D angiography demonstrated acceptable imaging quality for the detection of the VA perforating arteries. As the advantages of the radiological evaluation, the overall morphology of the arteries can be evaluated. The morphological characteristics could be well delineated and originally classified into terminal or longitudinal types in relation to their course and into ventral, dorsal, or dorsolateral types in relation to the location of their termination.

Regarding the relationship between the anatomical type of VA and the number of detectable perforating arteries, non–PICA-type VAs (i.e., the PICA arose from the AICA) gave off significantly higher numbers of perforating arteries than other types of VAs. The previous anatomical evaluations reported ASA itself and the proximal segment of PICA constantly gives off perforating arteries [13, 20]; however the anatomy of perforators from VA in relation to the origins of ASA and PICA was not fully discussed previously. Our result indicates that the endovascular trapping of non–PICA-type VAs might be associated with a risk of perforating artery occlusion and supports the higher incidence of ischemic complications in previous reports of trapping of this type of VA [6, 8]. Special attention should be paid to the existence of perforating arteries in the treatment of VADAs in non–PICA-type VAs. In such cases, the reconstructive techniques including the stent-assisted coil embolization and the flow-diverter stent placement might be alternative techniques to preserve the blood flow of the branches as well as the VAs [17–19, 23–27].

The detected perforating arteries were classified into three types (ventral, lateral, and dorsolateral) depending on their terminations and into two types (terminal and longitudinal) depending on their course (Figs. 1 and 2). A longitudinal type perforating artery originated from the PICA and/or the proximal segment of the intradural VA might correspond to the LSA in terms of its course. Lasjaunias et al. defined the LSA as originating from either the PICA or the intradural VA and running along the lateral aspect of the medulla posterior to the dentate ligaments and anterior to the posterior spinal nerve roots [28]. These authors also reported that the LSA rostrally anastomosed with the PICA branches and showed variations of the connections with not only the intracranial VA but also various origins of the PICA, including the extracranial VA and radicular arteries [28]. In the present study, most of the longitudinal type perforating arteries showed multiple origins at the PICA, VA, and C1 radicular artery. This result supports the idea that this type of perforating artery corresponds to the LSA. Regarding the terminations, all ventral types were terminal type perforators; in contrast, most of the dorsolateral types were longitudinal type perforators. This result clearly indicates the posterolateral territory of the blood supply from the LSA.

The distances between the VA union and the origins of the perforating arteries were significantly different for the ventral type, lateral type, and dorsolateral type. The ventral type perforators originated from the VA close to the union; in contrast, the dorsolateral type perforators originated from the VA distant from the union. The lateral type perforators originated from any segment of the VA. According to these results, impairment of blood flow in the perforators close to the VA union causes ischemia on the ventral (medial) side of the medulla, whereas impairment of blood flow in the perforators arising from the proximal side of the VA causes an infarction on the dorsolateral side.

The anatomical characteristics of the perforating arteries have been evaluated by radiological methods in a few studies. Lescher et al. evaluated the detailed imaging anatomy of basilar artery perforators and found that 3D DSA was able to display the perforating branches from the basilar artery [11]. Shimada et al. reported higher visualization of the perforating arteries in patients with VADAs using high-resolution cone-beam computed tomography (VasoCT; Philips Healthcare, Best, Netherlands) than conventional 3D DSA [29]. These recently developed angiographic imaging modalities allow us to reliably visualize tiny perforating arteries and evaluate their anatomy.

Our study had three main limitations. First, our study design was retrospective and involved only two centers. However, the number of patients was sufficient to discuss the anatomy in comparison with gross anatomical methods. Second, the reconstructed images did not allow for visualization of the brain parenchyma itself; therefore, it was difficult to evaluate the absolute anatomical relationships between the perforating arteries and medulla. Further evaluation using the reconstructed images combined with the multimodality fusion technique should be considered. Third, we did not have a gold standard, the gross anatomical information, to compare with the imaging anatomical descriptions.

Conclusion

Non–PICA-type VAs, in which the PICA arose from the AICA, gave off significantly higher numbers of perforating arteries. The anatomical configuration of the perforating arteries could be well delineated and classified according to their courses and locations of the terminations. The currently available angiographic systems and reconstructed images can facilitate visualization of small perforating arteries from the VAs.

Acknowledgments The authors would like to thank Dr. Akira Ito (Department of Neuroendovascular Therapy, Kohnan Hospital) for the clinical data collection, and Tomohiro Chiba, Yukiko Jinbo (Radiological technicians, Division of Radiology, Kohnan Hospital), and Naoki Yamamoto (Radiological technician, Diagnostic Imaging Center, Kurume University School of Medicine) for the radiological data collection.

Funding This study was financially supported by the Japanese Society of Neuroendovascular Therapy.

Compliance with ethical standards

Conflict of interest The authors declare that they have no conflict of interest.

Ethical approval All procedures performed in studies involving human participants were in accordance with the ethical standards of the institutional and/or national research committee and with the 1964 Helsinki declaration and its later amendments or comparable ethical standards. For this type of study, formal consent is not required.

Informed consent Written informed consent was obtained from all patients before procedures; however, the need for informed consent for this study was waived because of the retrospective study design.

References

1. Arnold M, Bousser MG, Fahrni G, Fischer U, Georgiadis D, Gandjour J, Enninger D, Sturzenegger M, Mattle HP, Baumgartneret RW (2006) Vertebral artery dissection: presenting findings and predictors of outcome. Stroke 37: 2499–2503
2. Mizutani T, Aruga T, Kirino T, Miki Y, Saito I, Tsuchida T (1995) Recurrent subarachnoid hemorrhage from untreated ruptured vertebrobasilar dissecting aneurysms. Neurosurgery 36:905–911
3. Yamada M, Kitahara T, Kurata A, Fujii K, Miyasaka Y (2004) Intracranial vertebral artery dissection with subarachnoid hemorrhage: clinical characteristics and outcomes in conservatively treated patients. J Neurosurg 101:25–30
4. Kurata A, Ohmomo T, Miyasaka Y, Fujii K, Kan S, Kitahara T (2001) Coil embolization for the treatment of ruptured dissecting vertebral aneurysms. AJNR Am J Neuroradiol 22:11–18
5. Kurata A, Yamada M, Ohmomo T, Hirayama H, Suzuki S, Miyasaka Y, Irikura K, Fujii K, Kitahara T (2001) The efficacy of coil embolization at the dissection site of ruptured dissecting vertebral aneurysms. Interv Neuroradiol 7:73–82
6. Endo H, Matsumoto Y, Kondo R, Sato K, Fujimura M, Inoue T, Shimiuz H, Takahashi A, Tominaga T (2013) Medullary infarction as a poor prognostic factor after internal coil trapping of a ruptured vertebral artery dissection. J Neurosurg 118:131–139
7. Hamada J, Kai Y, Morioka M, Yano S, Todaka T, Ushio Y (2003) Multimodal treatment of ruptured dissecting aneurysms of the vertebral artery during the acute stage. J Neurosurg 99:960–966
8. Aihara M, Naito I, Shimizu T, Matsumoto M, Asakura K, Miyamoto N, Toshimoto Y (2018) Predictive factors of medullary infarction after endovascular internal trapping using coils for vertebral artery dissecting aneurysms. J Neurosurg 129:107–113
9. Ikeda H, Imamura H, Mineharu Y, Tani S, Adachi H, Sakai C, Ishikawa T, Asai K, Sakai N (2016) Effect of coil packing proximal to the dilated segment on postoperative medullary infarction and prognosis following internal trapping for ruptured vertebral artery dissection. Interv Neuroradiol 22:67–75
10. Lescher S, Zimmermann M, Konczalla J, Deller T, Porto L, Seifert V, Berkefeld J (2016) Evaluation of the perforators of the anterior communicating artery (AComA) using routine cerebral 3D rotational angiography. J Neurointerv Surg 8: 1061–1066
11. Lescher S, Samaan T, Berkefeld J (2014) Evaluation of the pontine perforators of the basilar artery using digital subtraction angiography in high resolution and 3D rotation technique. AJNR Am J Neuroradiol 35:1942–1947
12. Antunović V, Mirčić A, Marinković S, Brigante L, Mališ M, Georgievski B, Aksić M (2017) Clinical significance of the cerebral perforating arteries. Pril (Makedon Akad Nauk Umet Odd Med Nauki) 38:19–29
13. Marinković S, Milisavljević M, Gibo H, Maliković A, Djulejić V (2014) Microsurgical anatomy of the perforating branches of the vertebral artery. Surg Neurol 61:190–197
14. Djulejić V, Marinković S, Milić V, Georgievski B, Rašić M, Aksić M, Puškaš L (2015) Common features of the cerebral perforating arteries and their clinical significance. Acta Neurochir 157:743–754
15. Iwai T, Naito I, Shimaguchi H, Suzuki T, Tomizawa S (2000) Angiographic findings and clinical significance of the anterior and posterior spinal arteries in therapeutic parent artery occlusion for vertebral artery aneurysms. Interv Neuroradiol 6:299–309
16. Kudo T, Iihara K, Satow T, Murao K, Miyamoto S (2007) Incidence of ischemic complications after endovascular treatment for ruptured dissecting vertebral artery aneurysms. Comparison between those arising proximal to and distal to the origin of the posterior inferior cerebellar artery. Interv Neuroradiol 13:157–162
17. Narata AP, Yilmaz H, Schaller K, Lovblad KO, Pereira VM (2012) Flow-diverting stent for ruptured intracranial dissecting aneurysm of vertebral artery. Neurosurgery 70:982–989
18. Cerejo R, Bain M, Moore N, Hardman J, Bauer A, Hussain MS, Masaryk T, Rasmussen P, Toth G (2017) Flow diverter treatment of intracranial vertebral artery dissecting pseudoaneurysms. J Neurointerv Surg 9:1064–1068
19. Chen JA, Garrett MC, Mlikotic A, Ausman JI (2019) Treatment of intracranial vertebral artery dissecting aneurysms involving the posterior inferior cerebellar artery origin. Surg Neurol Int 10:116
20. Kayaci S, Caglar YS, Bas O, Ozveren MF (2013) Importance of the perforating arteries in the proximal part of the PICA for surgical approaches to the brain stem and fourth ventricle - an anatomical study. Clin Neurol Neurosurg 115:2153–2158
21. Garcia-Gonzalez U, Cavalcanti DD, Agrawal A, Spetzler RF, Preulet MC (2012) Anatomical study on the "perforator-free zone": reconsidering the proximal superior cerebellar artery and basilar artery perforators. Neurosurgery 70:764–772
22. Grand W, Budny JL, Gibbons KJ, Sternau LL, Hopkins LN (1997) Microvascular surgical anatomy of the vertebrobasilar junction. Neurosurgery 40:1219–1223
23. Hijikata T, Baba E, Shirokane K, Tsuchiya A, Nomura M (2018) Dissecting vertebral artery aneurysm presenting regrowth after stent-assisted coil embolization in acute stage. J Clin Med Res 10: 527–530
24. Ishikawa T, Yamaguchi K, Anami H, Ishiguro T, Matsuoka G, Kawamata T (2016) Stent-assisted coil embolisation for bilateral vertebral artery dissecting aneurysms presenting with subarachnoid haemorrhage. Neuroradiol J 29:473–478

25. Liu J, Jing L, Zhang Y, Song Y, Wang Y, Li C, Wang Y, Mu S, Paliwal N, Meng H, Linfante I, Yang X (2017) Successful retreatment of recurrent intracranial vertebral artery dissecting aneurysms after stent-assisted coil embolization: a self-controlled hemodynamic analysis. World Neurosurg 97:344–350
26. Cho DY, Choi JH, Kim BS, Shin YS (2019) Comparison of clinical and radiologic outcomes of diverse endovascular treatments in vertebral artery dissecting aneurysm involving the origin of PICA. World Neurosurg 121:e22–e31
27. Hosogai M, Matsushige T, Shimonaga K, Kawasumi T, Kurisu K, Sakamoto S (2018) Stent-assisted coil embolization for ruptured intracranial dissecting aneurysms involving essential vessels. World Neurosurg 119:e728–e733
28. Lasjaunias P, Vallee B, Person H, Ter Brugge K, Chiu M (1985) The lateral spinal artery of the upper cervical spinal cord. Anatomy, normal variations, and angiographic aspects. J Neurosurg 63:235–241
29. Shimada K, Tanaka M, Kadooka K, Hadeishi H (2017) Efficacy of high-resolution cone-beam CT in the evaluation of perforators in vertebral artery dissection. Interv Neuroradiol 23:350–356